Molecular Cell
Article

Nucleosomes Are Context-Specific, H2A.Z-Modulated Barriers to RNA Polymerase

Christopher M. Weber,[1,3] Srinivas Ramachandran,[1] and Steven Henikoff[1,2,*]
[1]Division of Basic Sciences
[2]Howard Hughes Medical Institute
Fred Hutchinson Cancer Research Center, Seattle, WA 98109, USA
[3]Molecular and Cellular Biology Program, University of Washington, Seattle, WA 98195, USA
*Correspondence: steveh@fhcrc.org
http://dx.doi.org/10.1016/j.molcel.2014.02.014

SUMMARY

Nucleosomes are barriers to transcription in vitro; however, their effects on RNA polymerase in vivo are unknown. Here we describe a simple and general strategy to comprehensively map the positions of elongating and arrested RNA polymerase II (RNAPII) at nucleotide resolution. We find that the entry site of the first (+1) nucleosome is a barrier to RNAPII for essentially all genes, including those undergoing regulated pausing farther upstream. In contrast to the +1 nucleosome, gene body nucleosomes are low barriers and cause RNAPII stalling both at the entry site and near the dyad axis. The extent of the +1 nucleosome barrier correlates with nucleosome occupancy but anticorrelates with enrichment of histone variant H2A.Z. Importantly, depletion of H2A.Z from a nucleosome position results in a higher barrier to RNAPII. Our results suggest that nucleosomes present significant, context-specific barriers to RNAPII in vivo that can be tuned by the incorporation of H2A.Z.

INTRODUCTION

Eukaryotic transcription by RNA polymerase II (RNAPII) is highly regulated and occurs on a DNA template that is condensed into repeating nucleosome units, each consisting of 147 bp of DNA wrapped around an octamer of histone proteins. Nucleosomes regulate access of cellular machinery to DNA and are modified by incorporation of functionally distinct histone variants (Talbert and Henikoff, 2010). Transcription across nucleosomes has been extensively studied in vitro (Kulaeva et al., 2013). In this defined setting, nucleosomes present a physical barrier that causes backtracking/arrest of RNAPII, and this barrier cannot be efficiently overcome unless the nucleosome is destabilized either with high salt or ionic detergent. These studies typically use minimal components to reconstruct transcription, whereas transcription in vivo is regulated by many protein complexes that modify the nucleosomal barrier. In this more complex setting, the effect of canonical and variant nucleosomes on RNAPII elongation is unknown.

The primary approach to investigate transcription in vivo has been to map the position of RNAPII on genomic DNA. However, progress in the field has been limited by methodologies, such as chromatin immunoprecipitation (ChIP), that have insufficient resolution. Recently, single-nucleotide-resolution strategies for mapping RNAPII were introduced, but these have specific limitations for investigating the role of nucleosomes in transcription. Native elongating transcript sequencing (NET-seq) (Churchman and Weissman, 2011) maps both elongating and backtracked/arrested complexes. However, NET-seq requires solubilization of RNAPII complexes, which is typically far from complete under native conditions in metazoan cells (Kimura et al., 1999). Another strategy, Precision Nuclear Run-on sequencing (PRO-seq), maps elongation-competent RNAPII but cannot detect backtracked/arrested complexes and involves removal of chromatin proteins (Kwak et al., 2013).

In budding yeast, NET-seq detected barriers to RNAPII elongation over gene body nucleosomes, but these did not precisely match the consensus locations found in vitro (Bondarenko et al., 2006; Jin et al., 2010). Importantly, the transcription start site (TSS) overlaps the first nucleosome (+1) in budding yeast, preventing analysis of RNAPII elongation across this position (Rhee and Pugh, 2012). However, the +1 nucleosome might play an important role in transcriptional regulation (Cairns, 2009), and in most organisms the +1 nucleosome is found downstream of the TSS, which is relatively depleted of nucleosomes (Jiang and Pugh, 2009). The +1 nucleosome is a strong barrier to transcription in vitro (Nock et al., 2012). This barrier is partially relieved by TFIIS-mediated reactivation, implying that RNAPII backtracks after encountering the nucleosome. Using PRO-seq to map elongating *Drosophila* RNAPII in vivo, the effect of the +1 nucleosome or downstream nucleosomes on transcription was inconclusive (Kwak et al., 2013). Thus, it remains unclear whether the nucleosome barrier observed in vitro exists in vivo, mainly due to technical limitations of current techniques to map RNAPII.

In all eukaryotes, the +1 nucleosome and a few downstream nucleosomes of active genes are enriched for the histone variant H2A.Z (Bönisch and Hake, 2012). H2A.Z is incorporated outside of replication and is mostly essential for viability across eukaryotes (Zlatanova and Thakar, 2008). In budding yeast, H2A.Z deletion led to slower RNAPII elongation at a single fusion gene (Santisteban et al., 2011), while in vitro, human H2A.Z nucleosomes were completely refractory to transcription (Thakar

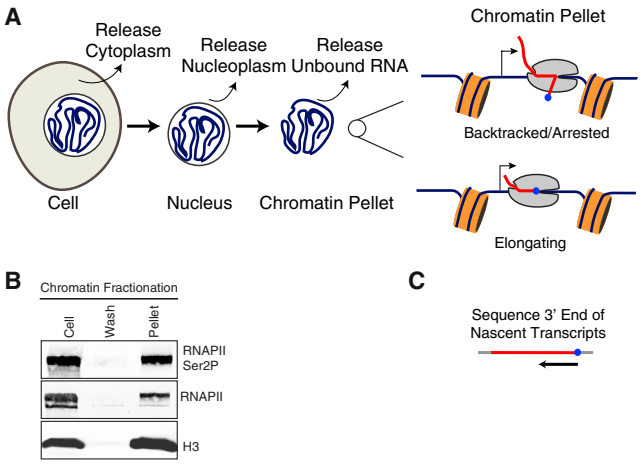

Figure 1. Approach to Comprehensively Capture RNAPII and Nascent RNA

(A) A gentle cellular fractionation scheme captures total bound RNAPII with nascent RNA, which is then sequenced to determine the precise 3′ end of nascent transcripts (blue dot). The protocol uses hypotonic buffers and nonionic detergents to release cytoplasm, nucleoplasm, and unbound RNA, capturing bound RNAPII complexes and nascent RNA in the insoluble chromatin pellet.

(B) A representative immunoblot of Ser2-phosphorylated RNAPII, RNAPII CTD, and H3 load control from whole-cell, cumulative wash, and final insoluble pellet fractions, showing high RNAPII recovery in the pellet.

(C) Nascent transcripts are extracted and their 3′ ends are determined by Illumina sequencing.

et al., 2010). Thus, the effect of H2A.Z on transcription across nucleosomes remains unclear.

Here we examine how RNAPII transcribes through nucleosomes in vivo and the effect of H2A.Z incorporation on RNAPII elongation. We describe a simple, generalizable strategy that comprehensively maps all forms of chromatin-bound RNAPII at nucleotide resolution without requiring transgenes, solubilization, or immunopurification. Using this strategy, we show that nucleosomes form context-specific barriers to transcription that can be tuned at least in part by incorporation of H2A.Z and provide insight into how RNAPII transcribes through nucleosomes in vivo.

RESULTS

Comprehensive Capture and Precise Strand-Specific Mapping of RNAPII

To comprehensively and precisely map total RNAPII, we took advantage of the extraordinary stability of the RNAPII ternary complex, which, once formed, remains bound to DNA in the presence of high salt, urea, detergents, and polyanions (Cai and Luse, 1987; Wuarin and Schibler, 1994). In metazoans, the complex is also highly insoluble even after nuclease digestion of genomic DNA (Kimura et al., 1999), precluding the use of NET-seq, which requires complete solubilization for RNAPII ChIP. Instead, we utilized the insolubility of RNAPII to purify the engaged complex and its attached nascent chain away from soluble RNA (Figure 1A). We quickly arrested transcription in *Drosophila* S2 cells with cold and used buffers containing nonionic detergents and EDTA to sequentially lyse the cell and the nucleus (Méndez and Stillman, 2000; Nishino et al., 2012; Wysocka et al., 2001), leaving an insoluble chromatin pellet with bound RNAPII and associated nascent RNA. Even though the ternary complex is resistant to harsh conditions, we sought to minimize bias associated with the release of unstable complexes by using minimally disruptive conditions. Using this protocol we successfully obtained comprehensive RNAPII recovery in the insoluble chromatin pellet (Figure 1B). We isolated nascent RNA from the insoluble pellet and selected for the presence of a 5′ 7-methylguanosine cap to further enrich for mRNA transcripts (Nechaev et al., 2010), and sequenced the 3′ end to determine the precise position of RNAPII using an established protocol (Churchman and Weissman, 2012) (Figure 1C). This approach provides strand-specific, reproducible maps of the active site of RNAPII at single nucleotide resolution (Figure 2A; see Figure S1 and Table S1 available online). A high correlation between the mapped strand of the 3′ end of nascent transcripts (3′NT) and the annotated gene model strand, in addition to a relatively uniform distribution of 3′NT signal between introns and exons, indicates that we are mapping nascent transcripts. Additionally, we observed a good correlation between the 3′NT read density and crosslinked ChIP-seq enrichment of RNAPII ($r = 0.69$) (Figure 2B). We also observed large 3′NT peaks at single positions, indicative of RNAPII stalling at individual positions during transcription. Thus, by this simple and general approach, we can comprehensively map RNAPII at nucleotide resolution, enabling investigation into the effect of nucleosomes on transcription.

Entry to the +1 Nucleosome Is a Major Barrier In Vivo

To obtain a global view of 3′NT signal from all transcripts, we plotted a 2D histogram of the normalized reads with respect to the TSS (Figure 2C). The highest 3′NT signal for most transcripts is within ~150 bp of the TSS and trails off to a relatively uniform distribution over downstream gene bodies. In *Drosophila* this roughly corresponds to the vicinity of the +1 nucleosome, but the exact position is variable (Mavrich et al., 2008; Weber et al., 2010). When we overlaid the nucleosome landscape derived from paired-end sequencing of DNA fragments protected from micrococcal nuclease digestion in nuclei (MNase-seq), we observed that the 3′NT signal is highest just upstream of the +1 nucleosome (Figures 2A and 2D).

As the highest density of 3′NT signal was found around the +1 nucleosome boundary, we asked where RNAPII tracks with respect to the +1 nucleosome of each transcript. First, we defined the precise position of the +1 nucleosome dyad for each transcript from paired-end MNase-seq landscapes. We then grouped transcripts into quartiles based on 3′NT reads over the flanking region (2 kb downstream of the TSS) and ordered transcripts in each quartile by the distance between their TSS and the dyad axis of their +1 nucleosome. The called dyad axis position can be clearly visualized on the MNase-seq heat map (Figure 3A), validating the accuracy of the called position (Table S2; Figure S2A). We next plotted the 3′NT heatmap with the same order of transcripts, which revealed a striking correspondence of 3′NT signal density with nucleosome positions.

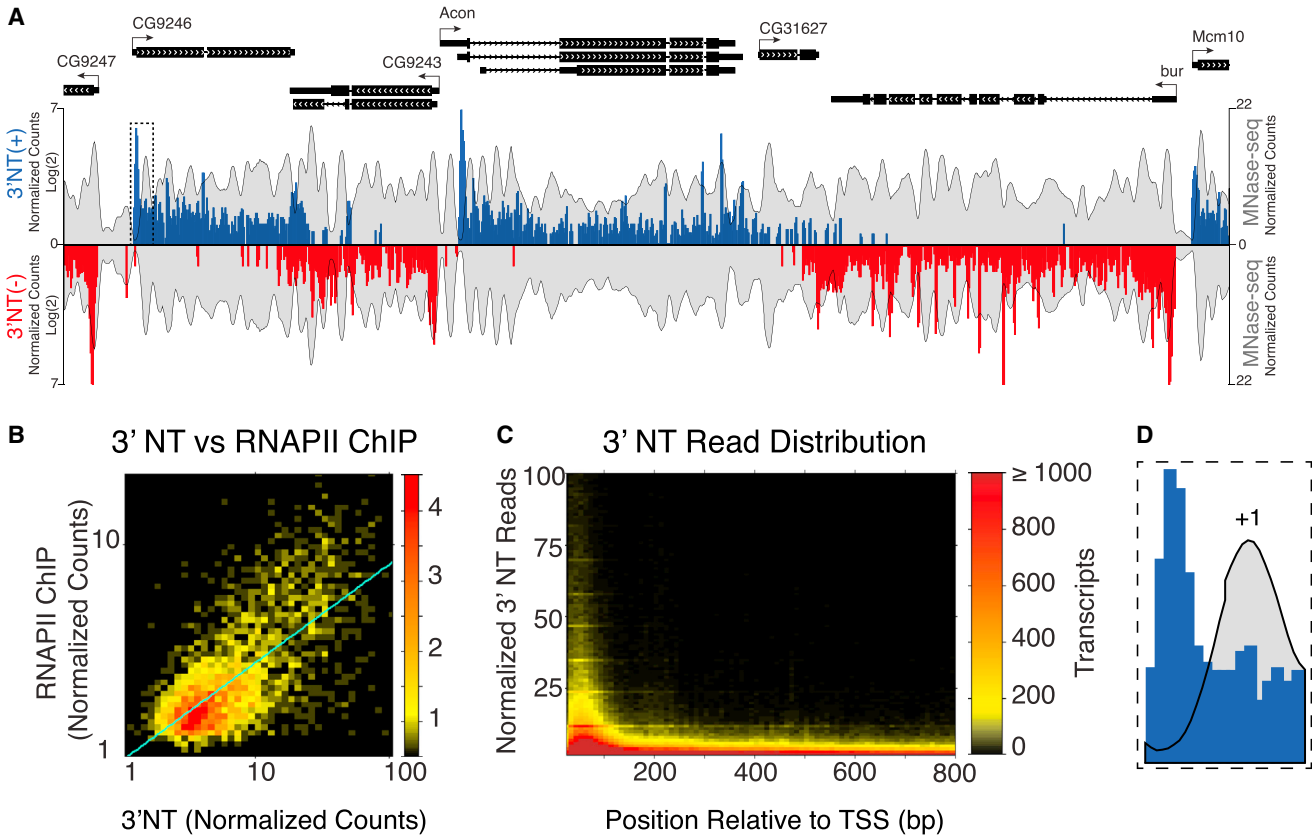

Figure 2. Precise Strand-Specific Mapping of Total RNAPII at Nucleotide Resolution

(A) A representative genome browser snapshot of highly expressed genes (Chr2L:21,162,558–21,180,500) showing the 3′ position of nascent transcripts (3′NT) that map to + (above axis, blue) and – (below axis, red) strands overlaid onto the nucleosome landscape map (mirrored, gray) derived from MNase-seq.

(B) Log-log density plot comparing our 3′NT reads with reads from RNAPII ChIP-seq (r = 0.69) (Core et al., 2012) aggregated from TSS to TSS+250 bp (normalized reads/bp).

(C) 2D histogram of 3′NT for all transcripts in the *Drosophila* genome plotted as a heatmap. All 3′NT and MNase-seq data are from two biological replicates.

(D) Boxed region shown in (A) at higher magnification.

Specifically, the leading edge of the 3′NT signal tracked with the entry site of the nucleosome (dyad - 73 bp) for +1 nucleosome positions independent of their distance from the TSS. This trend was observed for all quartiles, suggesting that this is an intrinsic effect of RNAPII encountering the +1 nucleosome, independent of the level of transcription and the nucleosome distance from the TSS.

In addition to the signal that aligns with the +1 nucleosome, we also observed 3′NT enrichment in the region between the TSS and +1 nucleosome entry site for many transcripts in the first quartile (Figure 3A, top). This high signal is likely due to promoter-proximal paused RNAPII (Adelman and Lis, 2012; Yamaguchi et al., 2013). To investigate this, we plotted the 3′NT signal for transcripts by degree of pausing, as defined by the change in RNAPII when negative elongation factor (NELF) is depleted (Gilchrist et al., 2010) (Figures S2B and S2C). We observed the highest 3′NT enrichment in the known region for paused polymerase at the most NELF-affected transcripts (~20–60 nt from the TSS). However, the leading edge of the 3′NT signal also tracked with the +1 nucleosome for all NELF-affected quartiles, similar to our observation for all genes. This suggests that apart from being subject to NELF-regulated pausing just downstream of the TSS, RNAPII stalls when it encounters the downstream +1 nucleosome.

We next sought to identify the position at the +1 nucleosome that is most refractory to RNAPII transit. The single-nucleotide resolution and high dynamic range of 3′NT enable us to observe individual spikes indicating consistent RNAPII stall sites. To characterize these positions, we define a stall as any single-nucleotide spike that is at least three standard deviations higher than the mean in a 200 bp window. We first investigated the probability of stalling (stall density) at positions relative to the +1 nucleosome dyad for genes grouped according to 3′NT quartiles as before. Averaging over thousands of transcripts, we observed a defined stall density peak at −80 bp from the dyad (Figure 3B; see also Figure S2D). Considering the 15–20 bp distance between the active site and the leading edge of RNAPII (Samkurashvili and Luse, 1996), the −80 bp stall position corresponds to the RNAPII leading edge positioned at −65 to −60 bp from the dyad or ~8–13 bp within the nucleosome. We observed a similar peak for all quartiles of average 3′NT signal, suggesting that this stall position is intrinsic to the

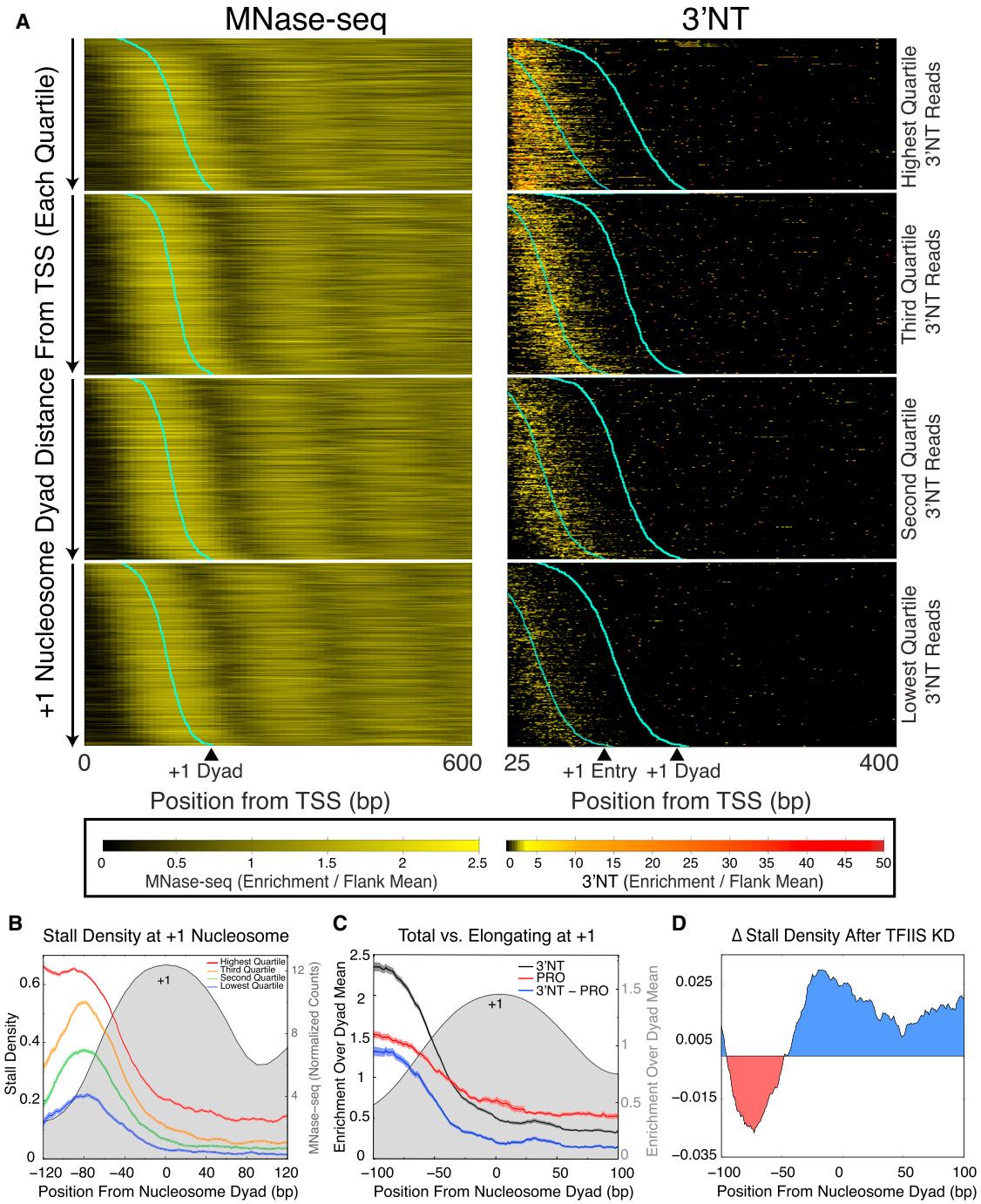

Figure 3. Entry to the +1 Nucleosome Is a Major Barrier In Vivo

(A) Transcripts (n = 3,981) were grouped into expression quartiles based on average 3′NT reads in the downstream flanking region (2 kb downstream of the TSS) and ordered from highest (top) to lowest quartile (bottom). Within each quartile, transcripts were arranged by distance between the TSS and the +1 nucleosome dyad axis (shortest to longest). Data within each quartile are shown as enrichment over the downstream flank mean (2 kb downstream of the TSS) for MNase-seq (left) and 3′NT (right). The called +1 dyad axis position for each transcript is overlaid onto normalized data for both MNase-seq and 3′NT. The calculated entry site (dyad axis position – 73 bp) is also shown for 3′NT (right).

(B) Stall density at the +1 nucleosome, grouped into expression quartiles based on the downstream flank mean (2 kb downstream of the TSS) of the transcripts, overlaid onto the +1 nucleosome (gray) from MNase-seq. Error bars calculated according to binomial distribution.

(C) Comparison between total RNAPII (3′NT) and elongation competent RNAPII (PRO = PRO-seq) for transcripts (n = 715) that met the coverage criterion in PRO-seq with respect to the dyad axis of the +1 nucleosome (gray) with plots of mean ± SEM.

(D) Change in stall density at the +1 nucleosome after depletion of TFIIS by RNAi.

physical barrier of the nucleosome. Thus, based on 3′NT signal tracking with the +1 nucleosome entry site, and mapping of the stall sites, we conclude that entry to the +1 nucleosome is a major barrier to transcription.

RNAPII Backtracks When It Stalls at Nucleosomes

In vitro, RNAPII has been shown to backtrack whenever there is an impediment to elongation (Komissarova and Kashlev, 1997; Nudler et al., 1997). If the entry site of the +1 nucleosome is a true barrier to RNAPII, then a fraction of RNAPII is expected to be backtracked, similar to observations in vitro (Kireeva et al., 2005). As our 3′NT signal maps both elongating and backtracked/arrested RNAPII, and PRO-seq captures only the elongating form, we can estimate the fraction of RNAPII that is backtracked by comparing 3′NT to published PRO-seq data for *D. melanogaster* S2 cells (Kwak et al., 2013). Because both methods entail quantitative recovery of nascent RNA and can be internally normalized for each transcript in the same way, we can subtract the PRO-seq enrichment at a given position from the 3′NT enrichment. If all bound RNAPII complexes are competent to elongate, we expect to see similar enrichment for 3′NT and PRO-seq. To estimate the extent of backtracking due to nucleosome barriers, we plotted 3′NT and PRO-seq relative to the dyad axis (Figure 3C; see also Table S3 and Figure S2E). We observed high enrichment up to −80 bp for 3′NT and PRO-seq, but 3′NT enrichment was ∼1.6 times higher. This suggests that a significant fraction of RNAPII is backtracked/arrested and unable to elongate in a run-on assay due to encountering the nucleosome barrier.

In order to directly determine whether stalled RNAPII that is unable to elongate in a run-on assay is backtracked, we used RNAi to deplete the transcript cleavage factor TFIIS from cells and mapped the resulting 3′NT positions. TFIIS stimulates RNA cleavage from backtracked RNAPII complexes, assisting in their reactivation (Sigurdsson et al., 2010). TFIIS knockdown did not change the position of the major barrier location at the +1 nucleosome (−80 bp from the dyad), as expected because TFIIS acts only after RNAPII backtracks (Figures S2F and S2G). Furthermore, TFIIS knockdown is unlikely to affect nucleosome positioning, because TFIIS action is limited to its effect on RNAPII, which has been shown in yeast and mammalian cells not to alter nucleosome positioning (Kouzine et al., 2013; Zhang et al., 2011). We have confirmed these results for *Drosophila* S2 cells, by showing that inhibition of transcriptional elongation has no effect on nucleosome positioning (Figure S2H).

TFIIS knockdown changed where RNAPII stalls, such that stalling decreased at the entry site and increased within the +1 nucleosome, closer to the dyad (Figures 3D and S2G). This increase within the nucleosome indicates that RNAPII unwraps the nucleosome to various degrees before backtracking to the nucleosome entry site, before RNA cleavage. Thus, RNAPII backtracks due to encountering a nucleosome barrier.

The Nucleosome Barrier Is Context Specific

The +1 nucleosome position is different from gene body nucleosomes because it is flanked by a nucleosome on only the downstream side. On the upstream side there is a nucleosome-depleted region, where the transcription machinery assembles before extending into productive elongation. The average distance between the TSS and the entry site of the +1 nucleosome (57 bp) is also considerably longer than the average length of linker DNA between downstream nucleosomes (20 bp). Hence, we asked if this distinction might also confer differences in how RNAPII transcribes through downstream nucleosomes relative to the +1 nucleosome. We found that the major barrier position at the +2 nucleosome was highly similar to that of the +1 nucleosome position (∼−80 bp), but with lower magnitude, and trailed slightly further into the nucleosome (Figure 4A). Thus, the barrier at −80 bp that we observed for the +1 nucleosome is not strictly due to being the first barrier to transcription or an effect of the promoter, as we observed this barrier position at the +2 nucleosome also. However, nucleosomes farther downstream displayed a barrier that is distinct from the +1 and +2 nucleosomes. In these gene body nucleosomes (>+2), RNAPII stalls upon entry (−80 bp), similar to the +1 and +2 nucleosomes, but also before the dyad axis (∼−50 and −20 bp). A similar trend was observed when we plotted the average of the 3′NT reads for these positions (Figure S3). Figure 4B summarizes the relative magnitude and the locations of the stalls relative to the leading edge of RNAPII's (active site +20 bp) position on the nucleosome. Thus, nucleosomes present unique stall signatures depending on their location downstream of the TSS.

Considering differences in how RNAPII transcribes through +1, +2, and gene body nucleosomes, we asked if the magnitude of the barrier is different at different nucleosome positions (Table S4). To measure the barrier, we calculated the fraction of positions that have a stall from 100 bp upstream of the dyad to the dyad (stall fraction, see Experimental Procedures). We also calculated the average 3′NT signal from 100 bp upstream of the dyad up to the dyad. We found that the +1 nucleosome position had the highest stall fraction and average 3′NT signal ahead of the dyad, indicating a higher barrier, whereas the downstream nucleosome positions were much less of a barrier and had relatively uniform magnitude (Figure 4C). Additionally, the higher stall fraction at +1 was highly similar for all +1 distances from the TSS, confirming that the increased barrier is due to the nucleosome and not skewed by proximity to the promoter (Figure 4D). These results suggest that once RNAPII clears the first major barrier, downstream elongation is less impeded, despite differences in the predominant location of the barrier within the nucleosome. We conclude that nucleosomes present a context-specific barrier to RNAPII, one in which nucleosome location relative to the TSS predicts the magnitude and characteristics of the barrier.

Nucleosomes Determine the Degree of RNAPII Stalling

If the +1 nucleosome indeed presents a physical barrier to RNAPII that leads to a defined stall position, then the degree of stalling should reflect nucleosome occupancy. To test this, we grouped transcripts based on the stall fraction and plotted the nucleosome occupancy, as determined by MNase-seq, with respect to the different stall fraction magnitudes. We observed a trend of increased +1 nucleosome occupancy with increased stall fraction (Figure 5A), indicating that nucleosome occupancy defines the extent of RNAPII stalling.

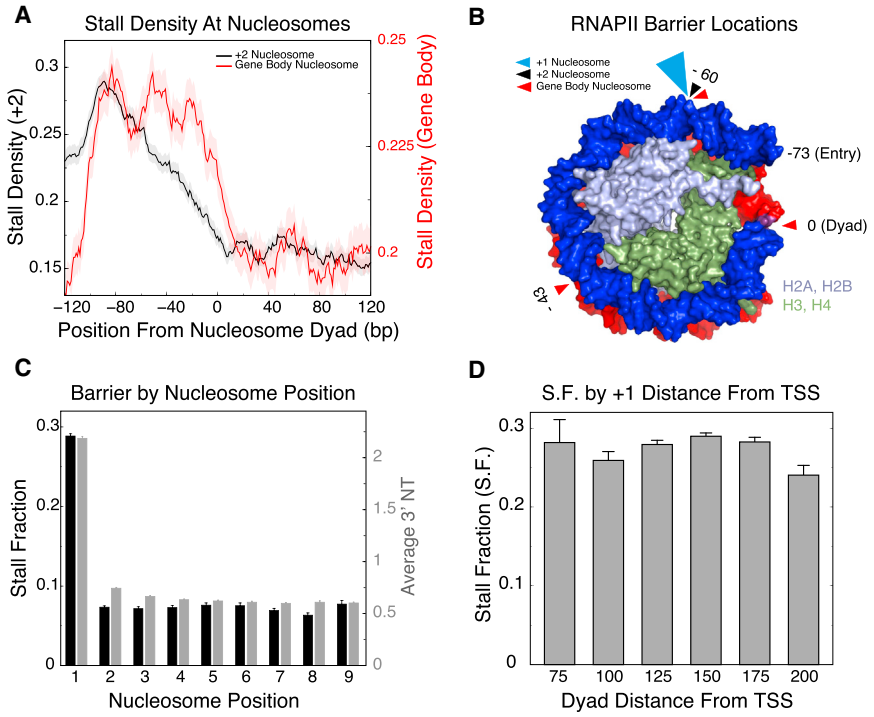

Figure 4. The Nucleosome Barrier Is Context Specific

(A) Comparison of RNAPII stall densities at +2 and gene body nucleosomes. Error bars calculated according to binomial distribution.

(B) Nucleosome structure with marked barrier locations for the leading edge of RNAPII that first encounters the nucleosome (barrier position detected by 3′NT + 20 bp). Size of arrowhead(s) reflects cumulative barrier magnitude relative to +1.

(C) Stall fraction and average 3′NT signal ahead of the dyad axis at nucleosome positions 1–9.

(D) Stall fraction (S.F.) is determined by the nucleosome and not proximity to the promoter, as S.F. is uniformly high for all dyad distances from the TSS. The mean ± SEM is plotted.

A unique feature of the +1 nucleosome and a few nucleosomes downstream is the conspicuous enrichment of H2A.Z (Mavrich et al., 2008; Weber et al., 2010). H2A.Z is incorporated into nucleosomes around promoters of active genes independent of replication, suggesting that H2A.Z might influence transcription (Cairns, 2009). Hence, we investigated H2A.Z occupancy of genes grouped according to stalled fraction. If H2A.Z does not influence RNAPII transit, then we expect genes with high +1 nucleosome occupancy to also have high H2A.Z and correlate with the extent of RNAPII stalling. In stark contrast, we find that absolute H2A.Z levels *anti*correlate with nucleosome occupancy and RNAPII stalling, such that genes with a lower stall fraction have higher H2A.Z levels and vice versa (Figure 5A). This suggests that where the extent of RNAPII stalling is less, H2A.Z is disproportionately increased.

The opposing trends of nucleosome occupancy and H2A.Z enrichment on stalling can also be seen by plotting average MNase-seq and H2A.Z ChIP-seq signal relative to the TSS for genes grouped according to stall fraction (Figure 5B). This trend is also clearly exemplified in individual gene tracks (Figure 5C), where high nucleosome occupancy and low H2A.Z lead to more stalled positions. Thus, increased nucleosome occupancy corresponds to increased RNAPII stalling at the +1 nucleosome, while increased H2A.Z occupancy correlates with decreased stalling, suggesting that the presence of H2A.Z eases the inhibitory effect of nucleosomes on transcription.

H2A.Z Modulates the Nucleosome Barrier to RNAPII

Our observations point to a role for H2A.Z in reducing the nucleosome barrier to RNAPII. To test this hypothesis, we depleted H2A.Z from chromatin using RNA interference (RNAi) against H2A.Z and YL-1. YL-1 is orthologous to budding yeast Swc2, a subunit of the Swr1 complex that binds H2A.Z, and is essential for ATP-dependent exchange of H2A with H2A.Z (Wu et al., 2005). H2A.Z depletion by impairing Swr1-dependent incorporation provides independent confirmation of direct H2A.Z knockdown and controls for potential phenotypes caused by Swr1 activity alone (Halley et al., 2010). Within the chromatin fraction, H2A.Z knockdown reduced protein levels to 12% and 13% of control, and YL-1 knockdown reduced H2A.Z levels to 64% and 62% for the two biological replicates (Figure 6A).

We then determined the genome-wide occupancy of the remaining H2A.Z by ChIP-seq and mapped the 3′NT positions in the knockdown cells. Strikingly, nucleosome positions with increased RNAPII stalling after H2A.Z knockdown had significantly less H2A.Z relative to positions where stalling was unchanged, for +1, +2, and gene body nucleosomes (Figure 6B; see also Figures S4 and S5). Importantly, this effect was graded in the YL-1 knockdown due to less-efficient H2A.Z depletion, leading to smaller effects at the +1 and +2 nucleosome positions. GO analysis shows that metabolic processes and catalytic activity genes were overrepresentated ($p < \sim 10^{-2}$–10^{-6}), as expected for the S2 cell line. These results indicate that an important function of H2A.Z is to modulate the elongation kinetics of RNAPII both at the +1 nucleosome and further into gene bodies, which helps to explain its enrichment around promoters in virtually all eukaryotes.

H2A.Z Occupancy Anticorrelates with H3-H4 Nucleosome Turnover

How might H2A.Z modulate RNAPII kinetics? We hypothesized that H2A.Z might make the nucleosome easier to disrupt when encountered by RNAPII. We tested this by measuring the nucleosome turnover defined by CATCH-IT (Deal et al., 2010; Teves and Henikoff, 2011) to see if turnover correlated with H2A.Z occupancy. Much to our surprise, we found the opposite, that the level of H2A.Z occupancy anticorrelated with complete nucleosome turnover (Figure 7A). CATCH-IT measures nucleosome turnover as the replacement of H3 and H4, but not H2A

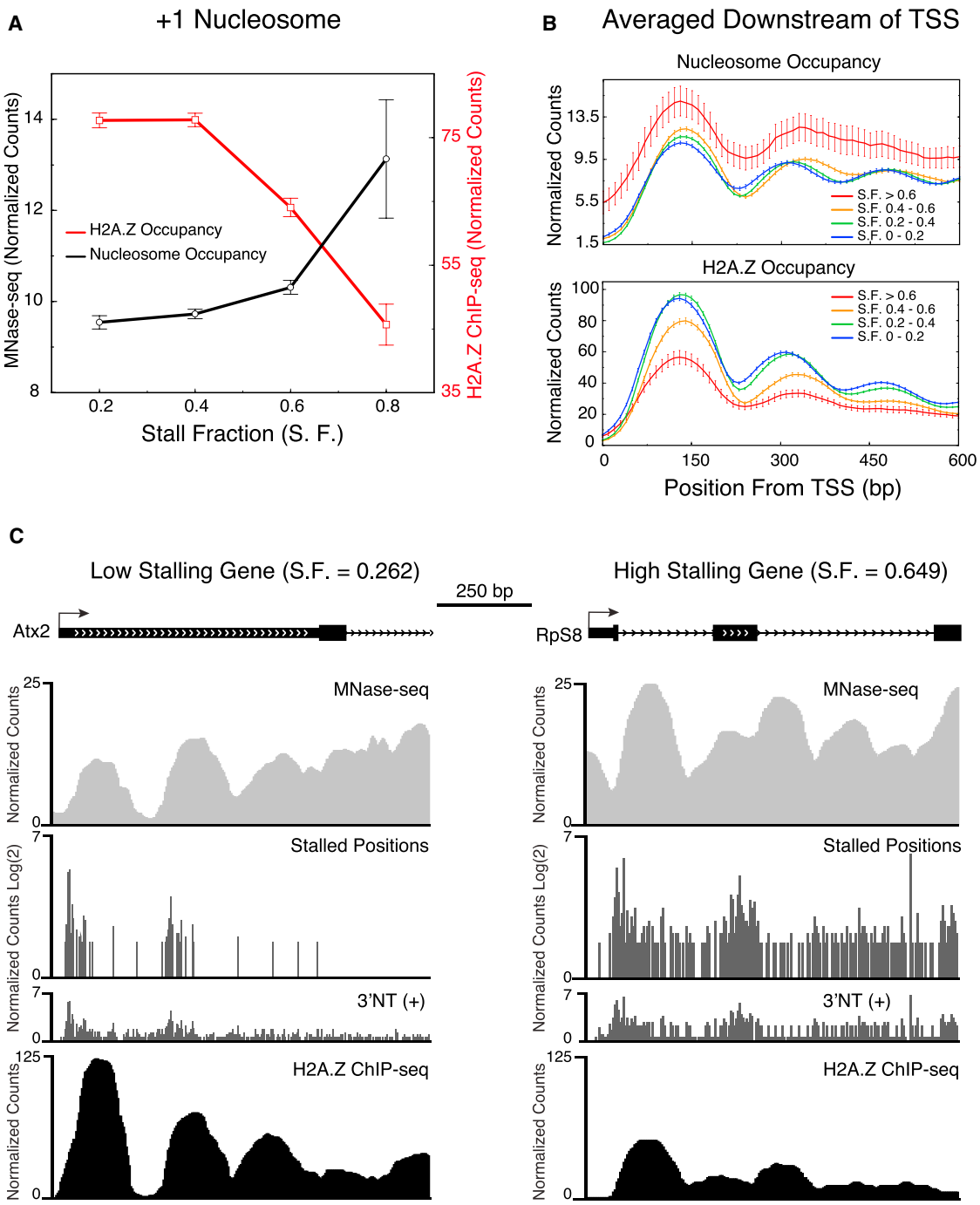

Figure 5. Nucleosomes Determine the Extent of RNAPII Stalling

(A) +1 nucleosome and H2A.Z occupancy at genes with different stall fraction (S.F.) magnitudes derived from the +1 nucleosome position (n = 3,981).

(B) MNase-seq and H2A.Z ChIP-seq normalized counts averaged over genes grouped by stall fraction (derived from +1 position) plotted relative to the TSS. Error bars represent SEM.

(C) UCSC Genome Browser snapshots for two genes with low stalling (left), showing low nucleosome occupancy (MNase-seq, top track) and high H2A.Z (bottom track), and high stalling (right), showing high nucleosome occupancy (above) and low H2A.Z (below), with the 3′NT normalized counts and stalled positions shown in between.

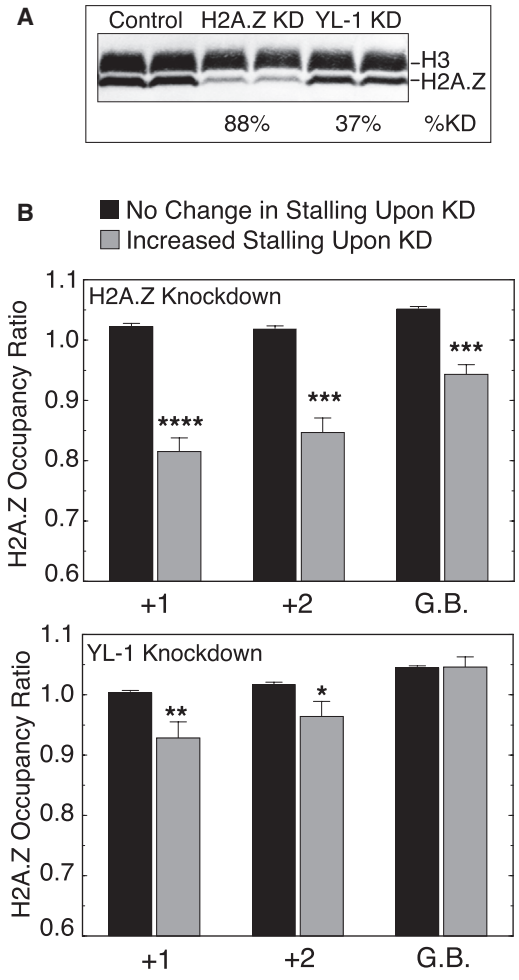

Figure 6. H2A.Z Modulates the Nucleosome Barrier to RNAPII

(A) Western blot showing the extent of H2A.Z depletion from chromatin after H2A.Z and YL-1 KD.

(B) Nucleosome positions with increased RNAPII stalling defined by 3′NT after knockdown have significantly less H2A.Z relative to unchanged positions (H2AZ KD, +1 n = 279, +2 n = 145, G.B n = 415; YL1 KD, +1 n = 124, +2 n = 98, G.B. n = 260). Asterisks represent statistically significant differences. The mean ± SEM is plotted.

or H2B, which suggests that H2A.Z-H2B dimers facilitate retention of $(H3\text{-}H4)_2$ tetramers.

DISCUSSION

Chromatin is the in vivo template for eukaryotic transcription; however, the fundamental process whereby RNAPII transcribes across a nucleosome is poorly understood. In vitro, RNAPII is known to behave as a Brownian ratchet, stalling at specific locations associated with strong histone-DNA contacts (Bintu et al., 2012; Selth et al., 2010), whereas in vivo a lack of suitable techniques has hampered understanding of this process. Using a simple technique that comprehensively maps total RNAPII at base-pair resolution in metazoan cells, we have gained fundamental insights into regulation of RNAPII elongation by nucleosomes. Our genome-wide map of the base-pair position at which the last RNA nucleotide is incorporated represents the ultimate metric of the process of transcription.

In vitro, the precise barrier position on a nucleosome template can be determined by the length of RNA produced (Kireeva et al., 2005). Under permissive conditions, a fraction of RNAPII can transcribe through the nucleosome, but smaller-length RNAs are produced when RNAPII encounters an insurmountable mechanical barrier, backtracks, and arrests. There is a consensus from a large body of work that +15 and +45 bp into the nucleosome are the major barrier positions (Bondarenko et al., 2006; Kulaeva et al., 2013). The leading edge of RNAPII encounters the nucleosome 15–20 bp in front of the active site where polymerization takes place (Samkurashvili and Luse, 1996), whereby the leading edge of RNAPII is around +35 and +65 bp into the nucleosome. These positions have been attributed to strong histone-DNA interactions and have been observed even in the presence of high salt and elongation factors such as TFIIS and FACT. Surprisingly, our comprehensive single-nucleotide-resolution maps of RNAPII in vivo reveal nucleosomal barriers that differ from the in vitro consensus. The consensus barrier position we find for all nucleosome positions is at −7 bp from the nucleosome entry site (−80 bp from the dyad axis), putting the leading edge of RNAPII at just +8 to +13 bp into the nucleosome, approximately a single helical turn of DNA. It is intriguing that the nature of the nucleosome barrier in vivo is so distinct from that in vitro. This distinction might be attributed to torsional constraint of the template in vivo but not in vitro, where the accumulation of positive supercoils ahead of RNAPII destabilizes nucleosomes (Sheinin et al., 2013; Teves and Henikoff, 2014). Hence, our data point to a different mechanism of RNAPII transit across nucleosomes in vivo compared to existing models using purified components and reconstituted nucleosomes.

Our analysis in vivo allows investigation into different nucleosome positions with respect to the TSS. We found that the overall magnitude of stalling is highest at the +1 nucleosome. Gene body nucleosomes also contain stalling positions further into the nucleosome, more closely resembling what has been observed in vitro (Kulaeva et al., 2013) and in budding yeast (Churchman and Weissman, 2011), albeit at much lower magnitude than is observed for the +1 nucleosome. It is possible that the relative lack of H2A.Z and/or histone modifications enriched on the +1 and +2 nucleosomes (Zentner and Henikoff, 2013) account for the closer resemblance of RNAPII transit at gene body nucleosomes to its action on unmodified canonical nucleosomes in vitro.

Arrested and/or backtracked RNAPII complexes detected by 3′NT account for ~60% of the total 3′NT signal at the nucleosome (Figure 3C) and are distinct from RNAPII that is found at the promoter-proximal paused position immediately downstream of the TSS. We observed the expected signal for paused RNAPII close to TSS, but we also observed RNAPII tracking with the nucleosome, similar to nonpaused genes. Thus, while an effect of the promoter sequence on pausing is clear (Kwak et al., 2013; Lagha et al., 2013), our results suggest that after RNAPII pause release the complex encounters a nucleosome barrier, which might contribute to promoter-proximal pausing (Mavrich et al., 2008). In addition, 3′NT detected barriers with a

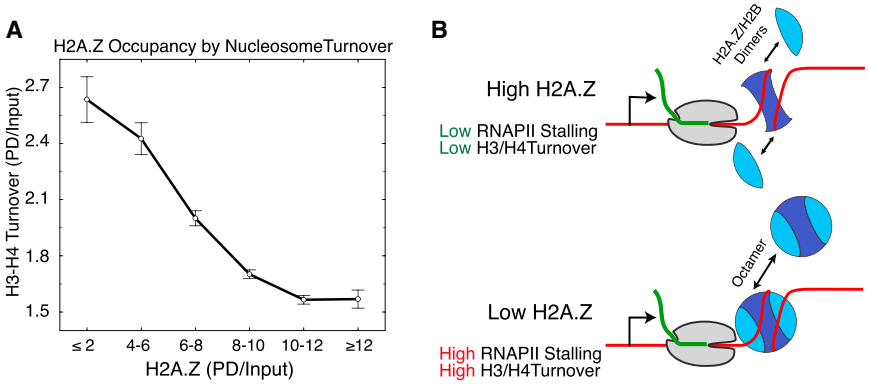

Figure 7. H2A.Z Occupancy Anticorrelates with H3-H4 Nucleosome Turnover

(A) H2A.Z occupancy anticorrelates with turnover of H3-H4 defined using CATCH-IT. The mean ± SEM is plotted.

(B) Model describes a likely mechanism for how H2A.Z reduces the barrier to RNAPII.

similar stall signature at downstream nucleosomes, where promoter-proximal pausing is not a complicating factor.

The +1 and +2 positions are much more highly enriched than gene body nucleosomes for H2A.Z, which is extensively acetylated on the N-terminal tail (Bruce et al., 2005; Valdés-Mora et al., 2012) and stimulates chromatin remodeler activity (Goldman et al., 2010). Wherever the barrier to RNAPII was increased after RNAi, we observed that H2A.Z levels were significantly decreased relative to unchanged positions. These observations are supported by results in yeast, where H2A.Z increased the elongation rate of RNAPII at a single fusion gene (Santisteban et al., 2011), and indicate that higher H2A.Z levels in gene bodies might influence expression of responsive genes (Coleman-Derr and Zilberman, 2012).

We were surprised by evidence suggesting that H2A.Z preserved $(H3\text{-}H4)_2$ tetramers during transcription, but this provided mechanistic insight into how H2A.Z might modulate the nucleosome barrier. Whereas many studies have investigated the stability of the H2A.Z-containing nucleosome, it remains unresolved whether H2A.Z stabilizes or destabilizes the intact nucleosome (Bönisch and Hake, 2012). However, in vivo results suggest that at dynamic regions of the genome where nucleosomes are disrupted, H2A.Z-containing nucleosomes are especially labile (Jin and Felsenfeld, 2007). The crystal structure of the H2A.Z nucleosome showed that a single amino acid difference in H2A.Z compared to H2A results in destabilization of its interaction with H3-H4 through its docking domain (Suto et al., 2000). We propose that when RNAPII enters the nucleosome, slightly unwrapping it, the H2A.Z-H2B dimer will be more easily lost, enhancing the elongation of RNAPII through nucleosomes (Figure 7B). By our model, when H2A.Z is low, RNAPII will stall more because the entire nucleosome must sometimes be removed. However, we cannot rule out the alternative possibility that $(H3\text{-}H4)_2$ tetramers with lower turnover rates are more likely to retain H2A.Z. In either case, the effect of H2A.Z manifests both at the +1 nucleosome and further into gene bodies and suggests that H2A.Z is most enriched where the barrier is largest, to assist in transcriptional elongation.

EXPERIMENTAL PROCEDURES

Cell Culture and RNAi

Drosophila S2-DRSC cells were obtained from the *Drosophila* Genomics Resource Center (Stock #181). Cells were cultured in Schneider's media supplemented with 10% heat-inactivated FBS at 25°C. dsRNA was synthesized using NEB reagents and protocols from PCR templates containing the T7 promoter sequence. PCR primers were as follows: H2Av forward (5′- TAATACGACTCACTA TAGGGCGAAACCGAATTCCGTAGAA - 3′), H2Av reverse (5′- TAATACGACTCACTATAGGGAGTAGGCCTGCGACAGA −3′), YL-1 (DRSC02765), GFP control (Hamada et al., 2005), and TFIIS (Adelman et al., 2005). To administer dsRNA, 2.5 × 10^6 log phase cells/cm^2 surface area were brought up in Schneider's without FBS (0.1mL/cm^2) and seeded to 25, 75, or 150 cm^2 flasks. A total of 30 μg dsRNA/1 × 10^6 cells was added to cells for 1 hr with intermittent mixing, an equal volume of Schneider's with 20% FBS was added, and cells were grown for 96 hr before harvesting.

Nascent RNA Isolation

We modified protocols from Nechaev et al. (2010), Nishino et al. (2012), and Wysocka et al. (2001) to fractionate cells and isolate nascent RNA. dsRNA-treated cells from 150 cm^2 flasks were harvested and pelleted by centrifugation for 1′ at 1,000 × g at 4°C. Cells were quickly washed with 2 mL ice-cold PBS supplemented with 10 μg/mL α-amanitin to inhibit transcription, were split into two separate 2 ml tubes, and were then pelleted by centrifugation 3′ at 3,000 × g. The cells were then lysed in 0.9 mL ice-cold buffer A (1 μl/mL SUPERase•In, protease inhibitor [Roche], 10 mM HEPES [pH 7.9], 10 mM KCl, 3 mM $MgCl_2$, 0.34 M sucrose, 10% glycerol, 1 mM DTT, 0.1% Triton X-100) supplemented with 10 μg/mL α-amanitin, 8′ on wet ice with intermittent mixing. Nuclei were then pelleted as before and brought up in 0.9 mL buffer B (1 μl/mL SUPERase•In, 9 mM EDTA, 0.2 mM EGTA, 1 mM DTT, protease inhibitor [Roche], 0.1% Triton X-100) 15′ on wet ice, and repeated twice or until nuclei lyse. The chromatin pellet was then brought up in 0.9 mL buffer B+ (1 μl/mL SUPERase•In, 20 mM EDTA, 0.2 mM EGTA, 2 mM spermine, 5 mM spermidine, 1 mM DTT, protease inhibitor [Roche]) and washed three times. The final insoluble pellet was brought up in 1 mL buffer B+ with 1% SDS, and aliquots were harvested to assay knockdown efficiency or for western analysis. Antibodies for western blots are as follows: RNAPII (ab817), phospho S2 RNAPII (ab5095), H3 (ab1791), H2Av (Active Motif #39715), and TFIIS (Adelman et al., 2005). The two pellets from the same original flask were pooled and dissolved in 10 mL Trizol, and RNA was isolated according to manufacturer's instructions. All RNA precipitation steps were conducted after incubation with 0.3 M NaOAc and GlycoBlue. Biological replicates were collected for each treatment.

Solexa Sequencing and Alignment

3′NT Library Preparation

Nascent RNA was treated with DNase (RQ1, Roche) and extracted with acid phenol and ethanol precipitated with GlycoBlue and 0.3 M NaOAc. We selected for the presence of a 5′ cap using Terminator 5′-Phosphate-Dependent Exonuclease (Epicenter), as described (Nechaev et al., 2010). Nascent, capped RNA was purified with acid phenol as before. Libraries were constructed as described for NET-seq (Churchman and Weissman, 2012) with the following modifications. Ligated RNA was digested with 2× alkaline fragmentation buffer at pH 10.3 for 30′. Reverse transcriptase primer concentration was reduced to 1.09 μM in RT reaction mix. Libraries were amplified with KAPA HiFi under limiting cycles. Following amplification, PCR reactions were purified with AMPure XP beads at a 1:1 ratio before PAGE purification to aid in the elimination of empty products. Biological replicates were sequenced for each condition.

Solexa libraries were subjected to cluster generation and 25 or 50 rounds of single-end sequencing using a unique sequencing primer (Churchman and Weissman, 2012). After processing and base calling by the Illumina Eland program, reads were first filtered by aligning with Bowtie 0.12.8 with default settings (with flag –best) against the reference noncoding RNA fasta file we created. This reference was created by taking the last 35 nt of each sequence in BDGP5.68. Unmapped reads were then aligned against Dmel 5.3 as before (Table S1).

MNase-seq and ChIP-seq

MNase-seq and ChIP-seq were performed as described (Weber et al., 2010) except without formaldehyde crosslinking, and chromatin was solubilized with 80 mM NaCl and needle extracted. Solexa libraries were constructed as previously described (Henikoff et al., 2011) with modifications. We used the TruSeq oligo design to enable barcoding of libraries with an AMPure XP to sample ratio of 1:1. Cluster generation and 25 rounds of paired-end sequencing by Illumina HiSeq 2000 were performed by the Fred Hutchinson Cancer Research Center Genomic and Shared Resource. Following processing and base calling by the Illumina Eland program, reads with zero, one, or two mismatches were mapped to Dmel 5.3 using Novoalign, and default parameters with multiple hits assigned to one location at random.

Data Analysis

The fraction of reads mapped at each nucleotide was multiplied by the total number of nucleotides mapped genome-wide to give a normalized count at that position. The 3′NT signal for each strand was normalized separately and was used at base-pair resolution (for 3′NT, each read was mapped to a single position, which corresponds to the 3′ end of the nascent transcript). 3′ exon end position was excluded from 3′NT analysis. MNase-seq and ChIP-seq reads were aggregated to ten base-pair windows, and only paired-end reads of length $\geq$76 and $\leq$160 bp were used. PRO-seq data sets were obtained from the GEO database, under accession number GSM1032758. The bedgraph file was parsed with each line as a read and normalized in an identical manner as 3′NT data.

Enrichment over the flank mean was calculated as follows: the flank for each fly transcript (identifier, FBtr# in flybase, database version Dme1 5.3) was from TSS to TSS+2,000 bp, unless interrupted by transcripts on the same or opposite strand. The minimum flank considered was 500 bp. For plots of average 3′NT (or PRO-seq) relative to the nucleosome dyad, we define the flank as Dyad−120 to Dyad+120. For 3′NT or MNase-seq data, the mean enrichment was calculated for each flank. When plotting 3′NT or MNase-seq for a given transcript, the enrichment at a given position was divided by the mean enrichment of the flank to enable comparison between different transcripts. For most analyses, only those transcripts that had nonzero flank mean were used. Expression quartiles were determined based on the flank mean of transcripts.

MNase-seq enrichment between TSS−2,000 and TSS+2,000 was used for calling dyad positions. A 20 point running average and the first derivative were calculated around each position. The definition of a peak was a point at which the derivative was between −0.04 and +0.04, around which the derivative changed from negative to positive and where the MNase-seq signal was higher than the mean + 0.5* (SEM). The mean and standard error are calculated from plus or minus ten positions around that point. If two peaks were within 100 bp, only the position with higher MNase-seq occupancy was retained as a peak. Comparison with DANPOS, an independent method (Chen et al., 2013), reveals that a majority of nucleosome positions are similar (Figure S2A).

To define stall positions, the mean and the standard deviation of the surrounding 200 bp are calculated (excluding stall positions). The position is defined as a stall if its 3′NT value is higher than the mean + 3* (SEM). Since the stall positions are to be excluded from the mean calculation at a given position, finding stalls is an iterative process: at each subsequent round of stall identification, stalls identified in the previous rounds are eliminated from mean calculation. This process is repeated until no new stalls are identified. The stall density is defined as fraction of transcripts having a stall at a given position relative to the nucleosome dyad. The stall fraction is defined as the fraction of stalls in a given region of a transcript, usually between dyad and dyad−100 bp.

Nucleosome occupancy and H2A.Z occupancy were calculated from MNase-seq and ChIP-seq data, respectively, based on the called nucleosome dyad position. Occupancy is the sum of normalized reads between dyad−80 and dyad+80 for a given nucleosome of a given transcript. To calculate changes in H2A.Z occupancy upon knockdown, the H2A.Z occupancy for various nucleosomes was calculated for the H2A.Z and YL1 knockdown cells. We observed the +1, +2, and gene-body nucleosome occupancy to have significant linear correlation between knockdown and control (Figures S5A and S5B), hence we transformed the knockdown occupancies based on the linear fits of nucleosome occupancy between control and knockdown. After the transformation, the ratio of H2A.Z occupancy between control and knockdown reflected the relative loss or gain of H2A.Z upon knockdown.

The 3′NT ratio of a given stretch of a transcript (between dyad−100 and dyad for a given nucleosome) is defined as the ratio of the sum of 3′NT reads in that stretch in the knockdown to the sum for the control. The 3′NT reads are normalized by the flank mean to enable comparison between different data sets. A similar ratio was also calculated for a window of 100 bp at defined positions from the TSS to generate the plot shown in Figure S5H.

ACCESSION NUMBERS

Genomic data presented in this work are available at Gene Expression Omnibus under accession number GSE49106.

SUPPLEMENTAL INFORMATION

Supplemental Information includes five figures and four tables and can be found with this article at http://dx.doi.org/10.1016/j.molcel.2014.02.014.

ACKNOWLEDGMENTS

We thank Stirling Churchman for sharing protocols; Karen Adelman for sharing unpublished data, TFIIS antibody, and protocols; and Jorja Henikoff for computational support. We thank Peter J. Skene, Takehito Furuyama, Ines A. Drinnenberg, and Steve Hahn for critical comments on the manuscript. This work was supported by the Howard Hughes Medical Institute and an NSF Graduate Research Fellowship awarded to C.M.W.

Received: July 8, 2013
Revised: November 4, 2013
Accepted: January 28, 2014
Published: March 6, 2014

REFERENCES

Adelman, K., and Lis, J.T. (2012). Promoter-proximal pausing of RNA polymerase II: emerging roles in metazoans. Nat. Rev. Genet. *13*, 720–731.

Adelman, K., Marr, M.T., Werner, J., Saunders, A., Ni, Z., Andrulis, E.D., and Lis, J.T. (2005). Efficient release from promoter-proximal stall sites requires transcript cleavage factor TFIIS. Mol. Cell *17*, 103–112.

Bintu, L., Ishibashi, T., Dangkulwanich, M., Wu, Y.Y., Lubkowska, L., Kashlev, M., and Bustamante, C. (2012). Nucleosomal elements that control the topography of the barrier to transcription. Cell *151*, 738–749.

Bondarenko, V.A., Steele, L.M., Ujvári, A., Gaykalova, D.A., Kulaeva, O.I., Polikanov, Y.S., Luse, D.S., and Studitsky, V.M. (2006). Nucleosomes can form a polar barrier to transcript elongation by RNA polymerase II. Mol. Cell *24*, 469–479.

Bönisch, C., and Hake, S.B. (2012). Histone H2A variants in nucleosomes and chromatin: more or less stable? Nucleic Acids Res. *40*, 10719–10741.

Bruce, K., Myers, F.A., Mantouvalou, E., Lefevre, P., Greaves, I., Bonifer, C., Tremethick, D.J., Thorne, A.W., and Crane-Robinson, C. (2005). The replacement histone H2A.Z in a hyperacetylated form is a feature of active genes in the chicken. Nucleic Acids Res. *33*, 5633–5639.

Cai, H., and Luse, D.S. (1987). Transcription initiation by RNA polymerase II in vitro. Properties of preinitiation, initiation, and elongation complexes. J. Biol. Chem. *262*, 298–304.

Cairns, B.R. (2009). The logic of chromatin architecture and remodelling at promoters. Nature *461*, 193–198.

Chen, K., Xi, Y., Pan, X., Li, Z., Kaestner, K., Tyler, J., Dent, S., He, X., and Li, W. (2013). DANPOS: dynamic analysis of nucleosome position and occupancy by sequencing. Genome Res. *23*, 341–351.

Churchman, L.S., and Weissman, J.S. (2011). Nascent transcript sequencing visualizes transcription at nucleotide resolution. Nature *469*, 368–373.

Churchman, L.S., and Weissman, J.S. (2012). Native elongating transcript sequencing (NET-seq). Curr. Protoc. Mol. Biol. *Chapter 4*, Unit 4.14, 11–17.

Coleman-Derr, D., and Zilberman, D. (2012). Deposition of histone variant H2A.Z within gene bodies regulates responsive genes. PLoS Genet. *8*, e1002988.

Core, L.J., Waterfall, J.J., Gilchrist, D.A., Fargo, D.C., Kwak, H., Adelman, K., and Lis, J.T. (2012). Defining the status of RNA polymerase at promoters. Cell Rep. *2*, 1025–1035.

Deal, R.B., Henikoff, J.G., and Henikoff, S. (2010). Genome-wide kinetics of nucleosome turnover determined by metabolic labeling of histones. Science *328*, 1161–1164.

Gilchrist, D.A., Dos Santos, G., Fargo, D.C., Xie, B., Gao, Y., Li, L., and Adelman, K. (2010). Pausing of RNA polymerase II disrupts DNA-specified nucleosome organization to enable precise gene regulation. Cell *143*, 540–551.

Goldman, J.A., Garlick, J.D., and Kingston, R.E. (2010). Chromatin remodeling by imitation switch (ISWI) class ATP-dependent remodelers is stimulated by histone variant H2A.Z. J. Biol. Chem. *285*, 4645–4651.

Halley, J.E., Kaplan, T., Wang, A.Y., Kobor, M.S., and Rine, J. (2010). Roles for H2A.Z and its acetylation in GAL1 transcription and gene induction, but not GAL1-transcriptional memory. PLoS Biol. *8*, e1000401.

Hamada, F.N., Park, P.J., Gordadze, P.R., and Kuroda, M.I. (2005). Global regulation of X chromosomal genes by the MSL complex in Drosophila melanogaster. Genes Dev. *19*, 2289–2294.

Henikoff, J.G., Belsky, J.A., Krassovsky, K., MacAlpine, D.M., and Henikoff, S. (2011). Epigenome characterization at single base-pair resolution. Proc. Natl. Acad. Sci. USA *108*, 18318–18323.

Jiang, C.Z., and Pugh, B.F. (2009). Nucleosome positioning and gene regulation: advances through genomics. Nat. Rev. Genet. *10*, 161–172.

Jin, C., and Felsenfeld, G. (2007). Nucleosome stability mediated by histone variants H3.3 and H2A.Z. Genes Dev. *21*, 1519–1529.

Jin, J., Bai, L., Johnson, D.S., Fulbright, R.M., Kireeva, M.L., Kashlev, M., and Wang, M.D. (2010). Synergistic action of RNA polymerases in overcoming the nucleosomal barrier. Nat. Struct. Mol. Biol. *17*, 745–752.

Kimura, H., Tao, Y., Roeder, R.G., and Cook, P.R. (1999). Quantitation of RNA polymerase II and its transcription factors in an HeLa cell: little soluble holoenzyme but significant amounts of polymerases attached to the nuclear substructure. Mol. Cell. Biol. *19*, 5383–5392.

Kireeva, M.L., Hancock, B., Cremona, G.H., Walter, W., Studitsky, V.M., and Kashlev, M. (2005). Nature of the nucleosomal barrier to RNA polymerase II. Mol. Cell *18*, 97–108.

Komissarova, N., and Kashlev, M. (1997). RNA polymerase switches between inactivated and activated states by translocating back and forth along the DNA and the RNA. J. Biol. Chem. *272*, 15329–15338.

Kouzine, F., Gupta, A., Baranello, L., Wojtowicz, D., Ben-Aissa, K., Liu, J., Przytycka, T.M., and Levens, D. (2013). Transcription-dependent dynamic supercoiling is a short-range genomic force. Nat. Struct. Mol. Biol. *20*, 396–403.

Kulaeva, O.I., Hsieh, F.K., Chang, H.W., Luse, D.S., and Studitsky, V.M. (2013). Mechanism of transcription through a nucleosome by RNA polymerase II. Biochim. Biophys. Acta *1829*, 76–83.

Kwak, H., Fuda, N.J., Core, L.J., and Lis, J.T. (2013). Precise maps of RNA polymerase reveal how promoters direct initiation and pausing. Science *339*, 950–953.

Lagha, M., Bothma, J.P., Esposito, E., Ng, S., Stefanik, L., Tsui, C., Johnston, J., Chen, K., Gilmour, D.S., Zeitlinger, J., and Levine, M.S. (2013). Paused Pol II coordinates tissue morphogenesis in the *Drosophila* embryo. Cell *153*, 976–987.

Mavrich, T.N., Jiang, C., Ioshikhes, I.P., Li, X., Venters, B.J., Zanton, S.J., Tomsho, L.P., Qi, J., Glaser, R.L., Schuster, S.C., et al. (2008). Nucleosome organization in the Drosophila genome. Nature *453*, 358–362.

Méndez, J., and Stillman, B. (2000). Chromatin association of human origin recognition complex, cdc6, and minichromosome maintenance proteins during the cell cycle: assembly of prereplication complexes in late mitosis. Mol. Cell. Biol. *20*, 8602–8612.

Nechaev, S., Fargo, D.C., dos Santos, G., Liu, L., Gao, Y., and Adelman, K. (2010). Global analysis of short RNAs reveals widespread promoter-proximal stalling and arrest of Pol II in Drosophila. Science *327*, 335–338.

Nishino, Y., Eltsov, M., Joti, Y., Ito, K., Takata, H., Takahashi, Y., Hihara, S., Frangakis, A.S., Imamoto, N., Ishikawa, T., and Maeshima, K. (2012). Human mitotic chromosomes consist predominantly of irregularly folded nucleosome fibres without a 30-nm chromatin structure. EMBO J. *31*, 1644–1653.

Nock, A., Ascano, J.M., Barrero, M.J., and Malik, S. (2012). Mediator-regulated transcription through the +1 nucleosome. Mol. Cell *48*, 837–848.

Nudler, E., Mustaev, A., Lukhtanov, E., and Goldfarb, A. (1997). The RNA-DNA hybrid maintains the register of transcription by preventing backtracking of RNA polymerase. Cell *89*, 33–41.

Rhee, H.S., and Pugh, B.F. (2012). Genome-wide structure and organization of eukaryotic pre-initiation complexes. Nature *483*, 295–301.

Samkurashvili, I., and Luse, D.S. (1996). Translocation and transcriptional arrest during transcript elongation by RNA polymerase II. J. Biol. Chem. *271*, 23495–23505.

Santisteban, M.S., Hang, M., and Smith, M.M. (2011). Histone variant H2A.Z and RNA polymerase II transcription elongation. Mol. Cell. Biol. *31*, 1848–1860.

Selth, L.A., Sigurdsson, S., and Svejstrup, J.Q. (2010). Transcript elongation by RNA polymerase II. Annu. Rev. Biochem. *79*, 271–293.

Sheinin, M.Y., Li, M., Soltani, M., Luger, K., and Wang, M.D. (2013). Torque modulates nucleosome stability and facilitates H2A/H2B dimer loss. Nat. Commun. *4*, 2579.

Sigurdsson, S., Dirac-Svejstrup, A.B., and Svejstrup, J.Q. (2010). Evidence that transcript cleavage is essential for RNA polymerase II transcription and cell viability. Mol. Cell *38*, 202–210.

Suto, R.K., Clarkson, M.J., Tremethick, D.J., and Luger, K. (2000). Crystal structure of a nucleosome core particle containing the variant histone H2A.Z. Nat. Struct. Biol. *7*, 1121–1124.

Talbert, P.B., and Henikoff, S. (2010). Histone variants—ancient wrap artists of the epigenome. Nat. Rev. Mol. Cell Biol. *11*, 264–275.

Teves, S.S., and Henikoff, S. (2011). Heat shock reduces stalled RNA polymerase II and nucleosome turnover genome-wide. Genes Dev. *25*, 2387–2397.

Teves, S.S., and Henikoff, S. (2014). Transcription-generated torsional stress destabilizes nucleosomes. Nat. Struct. Mol. Biol. *21*, 88–94.

Thakar, A., Gupta, P., McAllister, W.T., and Zlatanova, J. (2010). Histone variant H2A.Z inhibits transcription in reconstituted nucleosomes. Biochemistry *49*, 4018–4026.

Valdés-Mora, F., Song, J.Z., Statham, A.L., Strbenac, D., Robinson, M.D., Nair, S.S., Patterson, K.I., Tremethick, D.J., Stirzaker, C., and Clark, S.J. (2012). Acetylation of H2A.Z is a key epigenetic modification associated with gene deregulation and epigenetic remodeling in cancer. Genome Res. *22*, 307–321.

Weber, C.M., Henikoff, J.G., and Henikoff, S. (2010). H2A.Z nucleosomes enriched over active genes are homotypic. Nat. Struct. Mol. Biol. *17*, 1500–1507.

Wu, W.H., Alami, S., Luk, E., Wu, C.H., Sen, S., Mizuguchi, G., Wei, D., and Wu, C. (2005). Swc2 is a widely conserved H2AZ-binding module essential for ATP-dependent histone exchange. Nat. Struct. Mol. Biol. *12*, 1064–1071.

Wuarin, J., and Schibler, U. (1994). Physical isolation of nascent RNA chains transcribed by RNA polymerase II: evidence for cotranscriptional splicing. Mol. Cell. Biol. *14*, 7219–7225.

Wysocka, J., Reilly, P.T., and Herr, W. (2001). Loss of HCF-1-chromatin association precedes temperature-induced growth arrest of tsBN67 cells. Mol. Cell. Biol. *21*, 3820–3829.

Yamaguchi, Y., Shibata, H., and Handa, H. (2013). Transcription elongation factors DSIF and NELF: promoter-proximal pausing and beyond. Biochim. Biophys. Acta *1829*, 98–104.

Zentner, G.E., and Henikoff, S. (2013). Regulation of nucleosome dynamics by histone modifications. Nat. Struct. Mol. Biol. *20*, 259–266.

Zhang, Z., Wippo, C.J., Wal, M., Ward, E., Korber, P., and Pugh, B.F. (2011). A packing mechanism for nucleosome organization reconstituted across a eukaryotic genome. Science *332*, 977–980.

Zlatanova, J., and Thakar, A. (2008). H2A.Z: view from the top. Structure *16*, 166–179.